Ionization-excitation of helium by high-resolution $(e, 2e)$ spectroscopy and 4-body distorted-wave calculations

X. L. Chen,[1] A. L. Harris,[2] J. M. Li,[1] T. P. Esposito,[2] J. K. Deng,[1] and C. G. Ning[1,3,*]

[1]*Department of Physics, State Key Laboratory of Low-Dimensional Quantum Physics, Tsinghua University Beijing 100084, China*

[2]*Physics Department, Illinois State University, Normal, Illinois 61790, USA*

[3]*Collaborative Innovation Center of Quantum Matter, Beijing, China*

(Received 27 June 2014; published 1 October 2014)

We present experimental and theoretical results for electron-impact-induced ionization and excitation of helium atoms. Using a high-sensitivity and high-resolution $(e, 2e)$ spectrometer, we measured the differential cross sections of ionization-excitation of He to the $n = 1-5$ states of He^+ at an impact energy of 600 eV. The experimental results are compared with 4-body distorted wave (4DW) calculations and first Born approximation (FBA) calculations. It was found that 4DW can well describe the shapes of the cross sections of the ionization with a simultaneous excitation. The cross-section ratios of excited states $n = 2-5$ to the ground state $n = 1$ were underestimated by FBA and 4DW calculations, indicating the need for further improvement of the theoretical methods.

DOI: 10.1103/PhysRevA.90.042701 PACS number(s): 34.80.Dp

I. INTRODUCTION

In contrast to the profound theoretical knowledge based on very precise experimental data that has been achieved for the static structure of atoms and molecules, our knowledge for the dynamic problem is rather limited [1], even for a very simple system, such as the dynamics of the electron-impact ionization. Recently, the experimental techniques and theoretical methods have improved greatly for treating the ionization problem [2–12]. The helium atom, the simplest many-electron system with correlation effects that need to be taken into account, has been extensively explored as the target of electron-impact ionization [2–25]. The theory has reached a sufficient degree to describe the electron-impact ionization of helium with the residual ion He^+ at its ground state [3,5]. However, the ionization with simultaneous excitation of He still remains a considerable theoretical and computational challenge. To date, $(e, 2e)$ experimental and theoretical works for this process have mostly focused on the final He^+ ion states with $n = 2,3$ [7,13–16,23–25], primarily due to the small cross section involved and the demanding energy resolution needed for discriminating the different final ion states. The only exception is that of Bellm *et al.* who report the $(e, 2e)$ ionization-excitation of He for $n = 1-4$ with coplanar geometry [26].

The experimental and theoretical works of ionization-excitation of He have been excellently reviewed by Bellm *et al.* recently [26]. Here, we only briefly summarize the works performed under coplanar or noncoplanar scattering geometry under electron momentum spectroscopy (EMS) conditions of high impact energies and high-momentum-transfer collisions [27–31], which were also used in the present work. The early EMS experiments of the helium ionization and excitation process were performed by Cook *et al.* [18] and Lermer *et al.* [20] at the impact energy 1200 eV. Recently, our group [23] and Watanabe *et al.* [24] performed the experiment at impact energies that varied from 1000 to 4260 eV using a high-efficiency generation EMS spectrometer. The data with high statistical accuracy provided a more stringent test for the theoretical models. However, only the results of $n = 2,3$ were reported due to the limitation of the energy resolution. Recently, we have improved the energy resolution and angle resolution of our $(e, 2e)$ spectrometer [31,32], which makes it possible to measure the higher excited states.

II. THEORETICAL AND EXPERIMENTAL METHODS

In an $(e, 2e)$ reaction, an incident electron with known energy E_i and momentum $\vec{k}_i$ impacts the He atom, and the two outgoing electrons are detected in coincidence to determine their energies and momenta. The energy and momentum of the scattered projectile are noted as E_f and $\vec{k}_f$, and E_e and $\vec{k}_e$ for the ejected electron. Using the conservation of energy and momentum, we have

$$\vec{q} = \vec{k}_i - \vec{k}_f - \vec{k}_e, \tag{1}$$

$$E_b = E_i - E_f - E_e, \tag{2}$$

where $\vec{q}$ is the recoil momentum, and E_b is the binding energy. Our $(e, 2e)$ takes the symmetric noncoplanar geometry, in which the two outgoing electrons have equal energies ($E_f \approx E_e$) and equal polar angles ($\theta_f = \theta_e = 45^\circ$). ϕ is the relative azimuthal angle between the ejected electron and the momentum transfer from the projectile to the target atom (see Fig. 1). The recoil momentum q can be given by

$$q = \left\{ [k_i - \sqrt{2}k_f]^2 + \left[\sqrt{2}k_f \sin\left(\frac{\phi}{2}\right) \right]^2 \right\}^{1/2}. \tag{3}$$

In our high-resolution and high-efficiency spectrometer, the electron gun equipped with an oxide cathode generates a well collimated electron beam with a low-energy spread. The electron beam impacts the He gas sample, which is introduced through a gas tube. The double toroidal energy analyzers equipped with the two-dimensional position sensitive detectors are employed to measure the energies and angles of two outgoing electrons [31,32]. The energy resolution is 0.65 eV

*ningcg@tsinghua.edu.cn

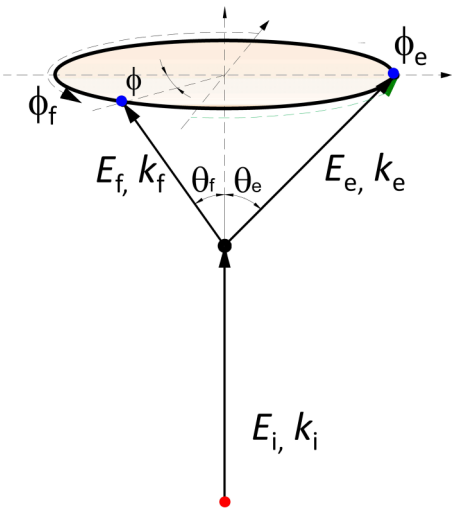

FIG. 1. (Color online) The noncoplanar sysmmetric geomety for studying $(e, 2e)$ reaction.

[full width at half maximum (FWHM)] at the impact energy of 600 eV and the azimuthal angle resolution $\Delta\phi = \pm 0.90^\circ$, the acceptance of polar angle $\Delta\theta = \pm 0.60^\circ$, which make it possible to measure the higher excited states.

In the present work, we report the differential cross sections of ionization-excitation of He for $n = 1-5$ and beyond at the impact energy of 600 eV plus the binding energy. The commercially available helium gas with a purity 99.995% was used, and the vacuum level was kept at 4×10^{-4} Pa during the measurements. The sample gas pressure in the reaction cell was estimated as 10^{-3} Pa accordingly. The experimental results were obtained by accumulations of data for 4 weeks to reach the good statistical accuracy. The experimental results are compared with 4-body distorted wave (4DW) calculations and first Born approximation (FBA) calculations [33]. The cross-section ratios of $n = 2,3,4,5$ to $n = 1$ are also reported in comparison with the theoretical calculations.

The full explanation of the 4-body distorted wave (4DW) and first Born approximation (FBA) models can be found in [33], and we present here only the necessary details. For both the 4DW and FBA models, the fully differential cross sections (FDCS) for electron-impact excitation-ionization of helium is given by

$$\frac{d^3\sigma}{d\Omega_1 d\Omega_2 dE_2} = \mu_{pa}\mu_{ie}\frac{k_f k_e}{k_i}|T_{fi}|^2, \tag{4}$$

where μ_{pa} is the reduced mass of the projectile and target atom, and μ_{ie} is the reduced mass of the He^+ ion and the ejected electron. The 4DW transition matrix T_{fi} is given by

$$T_{fi}^{4DW} = \left\langle \Psi_f^{4DW} \middle| V_i - U_i \middle| \Psi_i^{4DW} \right\rangle, \tag{5}$$

where Ψ_i^{4DW} is the initial-state wave function, Ψ_f^{4DW} is the final-state wave function, and $(V_i - U_i)$ is the perturbation. The initial-state Coulomb interaction between the incident projectile and the target atom is V_i, which is given by

$$V_i = \frac{-2}{r_1} + \frac{1}{r_{12}} + \frac{1}{r_{13}}, \tag{6}$$

where r_1 is the distance from the projectile to the target nucleus, r_{12} is the distance from the projectile to one target electron, and r_{13} is the distance from the projectile to the second target electron.

The initial-state wave function Ψ_i^{4DW} is written as a product of the incident projectile wave function $\chi_i(\vec{r}_1)$ and the target helium atom wave function $\Phi_i(\vec{r}_2,\vec{r}_3)$,

$$\Psi_i^{4DW} = \chi_i(\vec{r}_1)\Phi_i(\vec{r}_2,\vec{r}_3). \tag{7}$$

The final-state wave function is written as a product of the scattered projectile wave function $\chi_f(\vec{r}_1)$, the ejected electron wave function $\chi_e(\vec{r}_2)$, the residual He^+ ion wave function $\varphi_{nlm}(\vec{r}_3)$, and the postcollision Coulomb interaction (PCI) between the scattered projectile and the ejected electron $C(\vec{r}_{12})$. Then,

$$\Psi_f^{4DW} = \chi_f(\vec{r}_1)\,\chi_e(\vec{r}_2)\,\varphi_{nlm}(\vec{r}_3)\,C(\vec{r}_{12}). \tag{8}$$

For the target helium atom wave function, we use a 20-parameter Hylleraas wave function that includes both radial and angular correlations [34]. All continuum particle wave functions $\chi_i(\vec{r}_1), \chi_f(\vec{r}_1), \chi_e(\vec{r}_{12})$ are treated as distorted waves. The distorting potential used to calculate the incident projectile wave function is U_i, which is a static spherically symmetric Hartree-Fock potential that is a spherical approximation to V_i. Therefore, the term V_i–U_i in (5) represents the nonspherical part of the initial-state projectile–atom interaction. The distorting potential used to calculate the two final-state distorted waves is a spherically symmetric potential calculated from the final-state He^+ wave function.

The postcollision interaction is given by

$$C(\vec{r}_{12}) = \Gamma(1 - i\eta)\,e^{-\pi\eta/2}\,{}_1F_1(i\eta, 1, -ik_{12}r_{12} - i\vec{k}_{12}\cdot\vec{r}_{12}), \tag{9}$$

where Γ is the gamma function, η is the Sommerfeld parameter given here by $\eta = \frac{\mu_{pe}}{k_{12}}$, ${}_1F_1$ is a confluent hypergeometric function, and $\vec{k}_{12}$ is the relative momentum between the scattered projectile and the ejected electron. The final-state He^+ ion wave function $\varphi_{nlm}(\vec{r}_3)$ is simply a hydrogenic wave function with a nuclear charge of 2, for the specific n, l, m excited state being studied. We note that while we label electron 2 as the ionized electron and electron 3 as the bound He^+ electron, our actual calculations properly account for the indistinguishability of these two electrons by antisymmetrizing Ψ_f^{4DW}.

The FBA calculation also uses a 20-parameter Hylleraas wave function for the target helium atom, and treats the ionized electron as a distorted wave. However, the FBA model treats the incident and scattered projectiles as plane waves, and does not include the postcollision Coulomb interaction. Because the incident projectile is a plane wave in the FBA model, there is no initial-state distorting potential, making U_i equal to zero. Thus, the FBA T matrix is given by

$$T_{fi}^{FBA} = \left\langle \Psi_f^{FBA} \middle| V_i \middle| \Psi_i^{FBA} \right\rangle, \tag{10}$$

where

$$\Psi_i^{FBA} = \beta_i(\vec{r}_1)\,\Phi_i(\vec{r}_2,\vec{r}_3) \tag{11}$$

and

$$\Psi_f^{\mathrm{FBA}} = \beta_f(\vec{r}_1)\,\chi_e(\vec{r}_2)\,\varphi_{nlm}(\vec{r}_3)\,. \tag{12}$$

Here, $\beta(\vec{r})$ represents a plane wave and $\chi(\vec{r})$ represents a distorted wave. Comparison of the 4DW and FBA models shows that the two atomic electrons are treated exactly the same in both models, while the projectile interactions are treated differently. Specifically, in the FBA model, all projectile-target interactions are ignored, as is the postcollision Coulomb interaction between the projectile and ionized electron. Another significant difference in the two calculations is in the computational resources required for the calculations. The FBA model calculates a six-dimensional numerical integral, while the 4DW model calculates a nine-dimensional numerical integral, making the 4DW calculations very numerically intensive.

In the results presented here for excitation-ionization, the individual angular momentum state of the He^+ ion is not known. Therefore, theory must sum over all angular momentum and magnetic substates for a given n value. However, we have found that only the s and p states provide a meaningful contribution to the sum. The higher d, f, g, etc., states are three to six orders of magnitude smaller than the s and p states. Therefore, because the computational cost of these calculations is quite high, the sums shown here contain only the s and p states.

III. RESULTS AND DISCUSSION

Figure 2 shows the binding energy spectra at impact energy of $E_0 = 600$ eV plus binding energies, which were obtained by integrating all azimuthal angles ϕ. For extracting the differential cross-section for each He^+ ion state, the spectra at a series of angles ϕ were fitted by eight Gaussian peaks individually. The positions of those Gaussian peaks are the binding energies of the transition to $n = 1,2,3,4,5,6,7$ states of He^+, i.e., $E_b = 24.6, 65.4, 73.0, 75.6, 76.8, 77.5$, and 77.9 eV, respectively. A common width of 0.65 eV was used (FWHM) for all Gaussian functions. The Gaussian peak at 78.8 eV with a broader width (FWHM = 1.0 eV) is used to stand for the ionization intensity of the transitions to the higher than $n = 7$ of He^+ states but below the double ionization limits ($n = 8-\infty$). The solid line is the sum of these Gaussian peaks. Only the differential cross sections for $n = 1-5$ were individually compared to the theoretical calculations due to the smaller energy gaps and lower intensity for the higher states ($n \geqslant 6$).

Figure 3 shows the experimental differential cross sections in comparison with the theoretical calculations using the 4DW and FBA methods. The calculated intensities have been multiplied by a common factor for best fitting the experimental distribution because the experimental intensities are in a relative scale. The factor was globally used for the other peaks. It can be seen that the 4DW and FBA calculations have nearly identical shapes for $n = 1$, but the FBA is a factor of 1.25 larger than the 4DW calculation. This feature has been previously observed for single ionization [21,29,31]. For a better comparison of shapes, the FBA calculated intensity has been multiplied by a factor of 0.8. The use of distorted

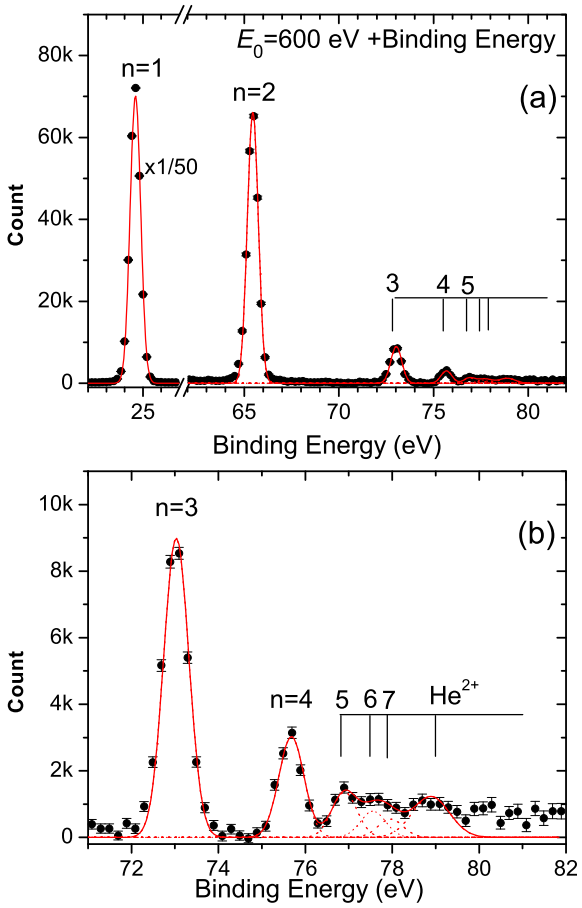

FIG. 2. (Color online) Binding energy spectra of He obtained at the impact energies of 600 eV plus binding energies. The intensity of peak $n = 1$ is scaled by a factor of 1/50 (a); an expanded view of the spectra in the energy range of 70–82 eV (b).

waves typically decreases the magnitude of the cross sections compared to the use of plane waves. There is a slight discrepancy between the FBA calculated distribution and the observed one for $n = 1$ when $\phi > 20^\circ$. However, the 4DW calculation is in excellent agreement with the experimental distribution. The difference is mainly due to the distorted wave effects. The larger angle ϕ means the larger recoil momentum, which is mainly contributed from the electron closer to the nucleus, thus is more easily influenced by the Coulomb potential. Generally, both 4DW and FBA calculations can provide a very good description of the differential cross-section for He^+ at its ground state ($n = 1$).

Figures 3(b)–3(e) show the differential cross section for the transition to $n = 2-5$ excited states of He^+. The scale factor for the theoretical results is the same as that used in Fig. 3(a). For the excited states, it is obvious that all calculations underestimate the experimental intensities. Nevertheless, the predicted shapes look similar to the experimental distributions. For a better comparison, the theoretical results were rescaled by another factor to better compare with the shape of the experimental distributions, as shown by the dashed lines (4DW in red, and FBA in blue). The rescaled factors were labeled in each panel. As Fig. 3(b) shows, after being multiplied by a factor of 1.73, the 4DW calculation better reproduces

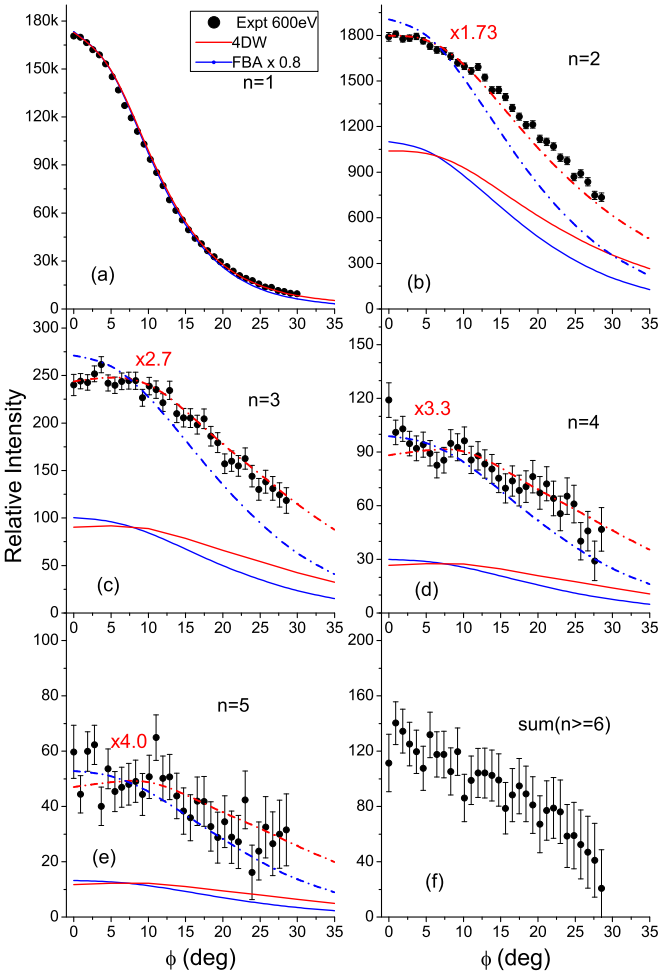

FIG. 3. (Color online) Differential cross sections for electron-impact ionization of He with a transition to the final-state He^+ with $n = 1$(a), $n = 2$ (b), $n = 3$(c), $n = 4$(d), $n = 5$(e), and $n = 6-\infty$ (f) at the impact energies of 600 eV plus binding energies. The solid theoretical curves were scaled by a common factor that was determined by best fitting the experimental distribution of $n = 1$. The dashed lines are the theoretical curves multiplied by another factor for comparing the shapes of calculated distributions with the measurements. See text for details.

the experimental distribution of $n = 2$, but there is still a significant discrepancy between the FBA calculation and experimental results. The predicted intensity by the FBA method declines too sharply as the angle ϕ increases. There is a similar situation for $n = 3$ except that a larger rescale factor of 2.7 is needed for the 4DW calculation. This underestimation gets worse with increasing n. The rescale factor became 3.3 for $n = 4$, and 4.0 for $n = 5$. This feature has also been previously observed with our 4DW calculations [24,26,27]. Previous calculations for single ionization and excitation-ionization using our 4DW and FBA models have shown that our models tend to predict cross sections that are too large for $n = 1$, and too small for $n > 1$ [29,31]. The magnitude discrepancies observed for $n > 1$ might be at least partially due to an overestimation of the $n = 1$ theoretical cross sections, which were used to normalize the experimental data. The summed intensity for $n \geqslant 6$ was plotted in Fig. 3(f). The 4DW and FBA calculations have not been conducted for comparison of $n \geqslant 6$ due to the very high computational cost.

Normalization issues aside, the shape agreement between experiment and theory is quite good, especially for the 4DW model. The FBA results fail to predict the relatively flat shape from $\phi = 0$ to $\phi = 10^\circ$, and also predict too sharp of a decline in the cross section as ϕ increases. At these projectile energies, the difference between a plane wave and a distorted wave treatment should be small, and the better shape agreement between the 4DW model and the experiment is most likely due to the inclusion of PCI. Specifically, for large ϕ, the two outgoing electrons are closer together than for smaller ϕ, making PCI more important at large ϕ. We confirmed that this is the case by performing a calculation using the 4DW model without PCI for the $n = 2$ case. This 4DW–no PCI calculation more closely resembled the FBA calculation at large ϕ.

Figure 4 allows us to more fully explore the magnitude discrepancies of the $n > 1$ cross sections because there are no normalization factors involved. The differential cross section for each excited state ($n = 2-5$) was divided by the differential cross section for $n = 1$. These ratios clearly show that both the

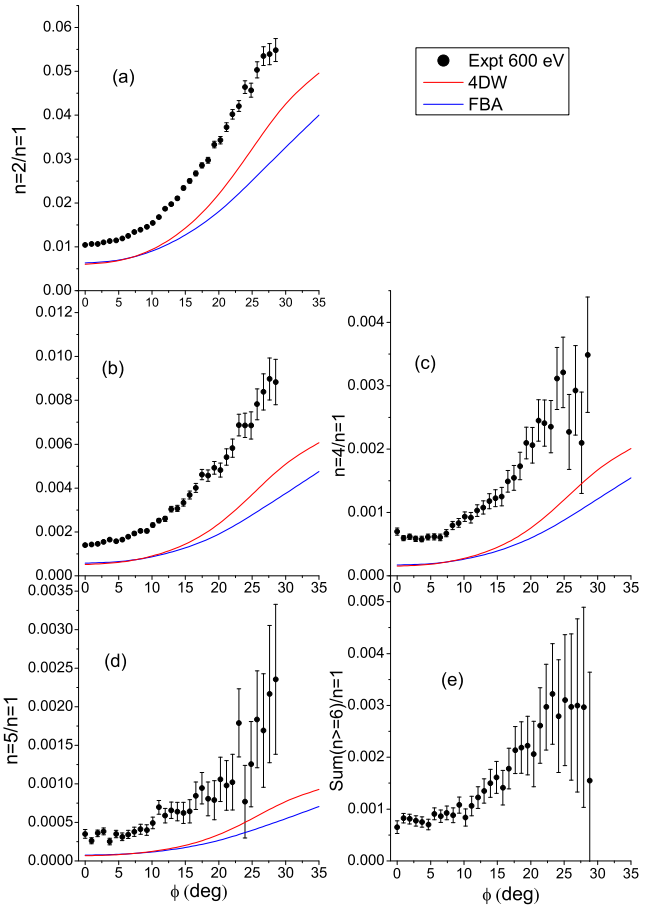

FIG. 4. (Color online) Differential cross-section ratios for ionization-excitation of He: $n = 2/n = 1$ (a), $n = 3/n = 1$(b), $n = 4/n = 1$(c), $n = 5/n = 1$(d), and sum$(n \geqslant 6)/n = 1$ (e). The theoretical ratios calculated using the 4DW (red line) and FBA (blue line) methods were plotted in comparison.

4DW and FBA models underestimate the experimental ratios. Again, this is something that has been observed before with our models [25,33,35], although the cause of the underestimation is still not understood. The discrepancies might be due to some effects that the 4DW and FBA have not included. The 4DW model more accurately predicts the shape of the experimental ratios, especially at large ϕ, which can again be attributed to the inclusion of PCI. It is interesting to note that Dal Cappello *et al.* calculated the differential cross sections using BBK (Brauner, Briggs, and Klar, also called the CCC method) model in comparison with the experimental results [15]. They individually normalized the data for comparing the shape of the cross section. Both BBK and our 4DW calculations can well describe the shapes. Moreover, the second-order Born-approximation (SBA) calculations by Watanabe *et al.* are in excellent agreement with the observed cross section for $n = 2$ at the impact energies 4260 and 2080 eV, and the agreement became worse at the impact energy 1240 eV. It should be noted that our FBA and 4DW models are known to have difficulty when ejected electron energies are low or the scattering angle is large [25,26,33], and both models lack second- and higher-order projectile-target interactions, which can be important for the excitation-ionization process. The present study clearly shows that there is still room for improving the theoretical models for calculating the ionization-excitation of helium.

IV. CONCLUSIONS

We presented the differential cross section for the ionization-excitation of helium using our high-resolution and high-sensitivity $(e, 2e)$ spectrometer at the impact energy of 600 eV. The experimental distributions were compared with the high-level 4DW calculations. It was found that both the 4DW and FBA theoretical methods can predict the shape of experimental distribution for He+ at its ground state ($n = 1$), but the 4DW method provides a much better description of experimental distributions for He^+ at its excited states ($n = 2-5$) than the FBA method does. Moreover, both 4DW and FBA methods underestimated the differential cross-section ratio for $n = 2/n = 1, n = 3/n = 1, n = 4/n = 1$, and $n = 5/n = 1$, and the underestimation gets worse as n increases. We hope that the present work will stimulate further theoretical work with more accurate descriptions of the challenging Coulomb 4-body problem.

ACKNOWLEDGMENTS

This work is supported by National Natural Science Foundation of China (NSFC) (Grants No. 11174175 and No. 91336104) and Ministry of Science and Technology of China (MOST) (Grant No. 2013CB922004) of the National Key Basic Research Program of China, and by the Tsinghua University Initiative Scientific Research Program.

[1] J. Ullrich, R. Moshammer, A. Dorn, R. Dörner, L. Ph. H. Schmidt, and H. Schmidt-Böcking, Rep. Prog. Phys. **66**, 1463 (2003).
[2] I. E. McCarthy and J. Mitroy, Phys. Rev. A **34**, 4426 (1986).
[3] A. Kheifets, I. Bray, A. Lahmam-Bennani, A. Duguet, and I. Taouil, J. Phys. B **32**, 5047 (1999).
[4] G. Sakhelashvili, A. Dorn, C. Höhr, J. Ullrich, A. S. Kheifets, J. Lower, and K. Bartschat, Phys. Rev. Lett. **95**, 033201 (2005).
[5] Z. J. Chen and D. H. Madison, J. Phys. B **38**, 4195 (2005).
[6] E. Ali, A. L. Harris, J. Lower, E. Weigold, C. G. Ning, and D. H. Madison, Phys. Rev. A **89**, 062713 (2014).
[7] O. Zatsarinny and K. Bartschat, J. Phys. B **47**, 061001 (2014).
[8] M. J. Ambrosio, G. Gasaneo, and F. D. Colavecchia, Phys. Rev. A **89**, 012713 (2014).
[9] X. Ren, A. Senftleben, T. Pflüger, A. Dorn, J. Colgan, M. S. Pindzola, O. Al-Hagan, D. H. Madison, I. Bray, D. V. Fursa, and J. Ullrich, Phys. Rev. A **82**, 032712 (2010).
[10] M. Dürr, A. Dorn, J. Ullrich, S. P. Cao, A. Czasch, A. S. Kheifets, J. R. Götz, and J. S. Briggs, Phys. Rev. Lett. **98**, 193201 (2007).
[11] M. Dürr, C. Dimopoulou, B. Najjari, A. Dorn, and J. Ullrich, Phys. Rev. Lett. **96**, 243202 (2006).
[12] X. G. Ren, A. Dorn, and J. Ullrich, Phys. Rev. Lett. **101**, 093201 (2008).
[13] X. Ren, I. Bray, D. V. Fursa, J. Colgan, M. S. Pindzola, T. Pflüger, A. Senftleben, S. Xu, A. Dorn, and J. Ullrich, Phys. Rev. A **83**, 052711 (2011).
[14] D. A. Horner, C. W. McCurdy, and T. N. Rescigno, Phys. Rev. A **71**, 010701(R) (2005).
[15] C. Dal Cappello, A. C. Roy, X. G. Ren, and R. Dey, Nucl. Instrum. Methods Phys. Res., Sect. B **266**, 570 (2008).
[16] G. Sakhelashvili, A. Dorn, C. Höhr, J. Ullrich, A. S. Kheifets, J. Lower, and K. Bartschat, Phys. Rev. Lett. **95**, 033201 (2005).
[17] A. Lahmam-Bennani, H. F. Wellenstein, C. Dal Cappello, M. Rouault, and A. Duguet, J. Phys. B **16**, 2219 (1983).
[18] J. P. D. Cook, I. E. McCarthy, A. T. Stelbovics, and E. Weigold, J. Phys. B **17**, 2339 (1984).
[19] A. Lahmam-Bennani, A. Duguet, C. Dupre, and C. Dal Cappello, J. Electron Spectrosc. Relat. Phenom. **58**, 17 (1992).
[20] N. Lermer, B. R. Todd, N. M. Cann, C. E. Brion, Y. Zheng, S. Chakravorty, and E. R. Davidson, Can. J. Phys. **74**, 748 (1996).
[21] Y. H. Fang and K. Bartschat, J. Phys. B **34**, L19 (2001).
[22] A. L. Godunov, C. T. Whelan, and H. R. J. Walters, Phys. Rev. A **78**, 012714 (2008).
[23] X. G. Ren, C. G. Ning, J. K. Deng, G. L. Su, S. F. Zhang, Y. R. Huang, and G. Q. Li, Phys. Rev. A **72**, 042718 (2005).
[24] N. Watanabe, M. Takahashi, Y. Udagawa, K. A. Kouzakov, and Yu. V. Popov, Phys. Rev. A **75**, 052701 (2007).
[25] S. Bellm, J. Lower, E. Weigold, I. Bray, D. V. Fursa, K. Bartschat, A. L. Harris, and D. H. Madison, Phys. Rev. A **78**, 032710 (2008).
[26] S. Bellm, J. Lower, K. Bartschat, X. Guan, D. Weflen, M. Foster, A. L. Harris, and D. H. Madison, Phys. Rev. A **75**, 042704 (2007).
[27] I. E. McCarthy and E. Weigold, Rep. Prog. Phys. **54**, 789 (1991).
[28] M. A. Coplan and J. H. Moore, Rev. Mod. Phys. **66**, 985 (1994).
[29] E. Weigold and I. E. McCarthy, *Electron Momentum Spectroscopy* (Kulwer Academic, New York, 1999).
[30] C. E. Brion, Int. J. Quantum Chem. **29**, 1397 (1986).

[31] C. G. Ning, S. F. Zhang, J. K. Deng, K. Liu, Y. R. Huang, and Z. H. Luo, Chin. Phys. B **17**, 1729 (2008).
[32] X. G. Ren, C. G. Ning, J. K. Deng, S. F. Zhang, G. L. Su, F. Huang, and G. Q. Li, Rev. Sci. Instrum. **76**, 063103 (2005).
[33] A. L. Harris, M. Foster, C. Ryan-Anderson, J. L. Peacher, and D. H. Madison, J. Phys. B **41**, 135203 (2008).
[34] J. F. Hart and G. Herzberg, Phys. Rev. **106**, 79 (1957).
[35] A. L. Harris, B. Milum, and D. H. Madison, Phys. Rev. A **84**, 052718 (2011).